



Review of the analytical network-averaging: part I — theoretical foundation

Mikhail Itskov¹ · Vu Ngoc Khiêm¹

Received: 15 April 2024 / Accepted: 6 May 2024
© The Author(s) 2024

Abstract

The analytical network-averaging, an elegant homogenization scheme, has been proposed in Khiêm and Itskov (*J. Mech. Phys. Solids* 95:254–269, 2016) to capture a wide range of mechanical phenomena in soft materials. These phenomena include nonlinear elasticity observed in unfilled rubbers, anisotropic damage behaviors in mechanoresponsive elastomers, phase transition occurring in natural rubbers, cross-effect of damage in double-network hydrogels, and irreversible fiber sliding in textile reinforcements. While the effectiveness of the analytical network-averaging has been evidenced through various illustrative examples, a thorough exposition of the theory remains elusive, primarily due to the concise nature preferred in conventional scientific articles and the specific thematic emphasis of individual publications. In the first part of this review series, an exhaustive theoretical examination of the analytical network-averaging concept is provided. Such theory postulates the presence of an orientational distribution function of material directions, such as fibers or polymer chains. Utilizing this distribution function, microscopic strain measures essential for solving homogenized boundary value problems can be obtained by averaging of macroscopic strain measures. It is interesting that in all scenarios, analytical derivation of the microscopic strain measures can always be obtained. Thus, such analytical homogenization scheme offers physically based invariants that automatically guarantee realistic behaviors (such as non-affine deformation, material objectivity and material symmetry) in stress response functions. This is particularly important in the age of data science and machine learning as it allows for the choice of stress hypothesis without limitations, while ensuring a priori interpretability of results.

Keywords Analytical network-averaging · Homogenization · Non-affine deformation · Interpretability · Internal variables · Nonlinear elasticity

1 Introduction

Soft materials refer to a class of solids that can be easily deformed when subjected to external stimuli. These materials encompass a wide range of substances, including polymers, colloids, biological macromolecules and textile reinforcements. One of the defining features of soft materials is their network structure, which gives rise to fascinating mechanical properties such as considerable stretchability or drapability. To ensure that soft materials meet the specific mechanical requirements for their intended applications, the network structure properties should be carefully engineered. This highlights the importance of employing physically based modeling approaches in optimization of soft materials, which helps avoid the resource-intensive nature of traditional trial-and-error procedures. Nevertheless, the heterogeneous nature of the network structure inherent in

✉ Vu Ngoc Khiêm
khiem.vu@rwth-aachen.de

¹ Department of Continuum Mechanics, RWTH Aachen University, Eilfschornsteinstr. 18, Aachen 52062, Germany

soft materials leads to non-affine deformation, thereby posing challenges for the development of physically based constitutive modeling of such materials.

To date, numerous homogenization schemes have been proposed for soft materials. They can be classified into two subcategories based on the characteristic of their random variables. The first type is the discrete homogenization approach, often referred to as the FE² method. In such method, the inherent material heterogeneities are modeled using a representative volume element (RVE). This approach involves the simultaneous solution of two sets of equations: one requires a finite element (FE) analysis conducted on the macroscopic structure using a coarse mesh, while the other entails a finite element computation performed on the RVE embedded within the macroscopic elements (see, for instance, [2, 3]). The macroscopic deformation gradient at the coarse scale is utilized to prescribe boundary conditions to the RVE. The upscaling is achieved through the Hill-Mandel condition [4, 5], resulting in a macroscopic stress as the averaging of the microscopic analog over the RVE. Although the FE² method is generally applicable to materials with periodic or statistically homogeneous microstructures, its discrete nature necessitates significant computational resources. On the other hand, the continuous homogenization approach leverages the network structure of soft materials to perform mathematical averaging. Many of these methodologies assume that the homogenized stretch serves as the only kinematic measure for the boundary value problem of soft materials. Beatty [6] assumed

isotropic distribution of polymer chains which facilitates an analytical solution for the average stretch $\bar{\Lambda} = \sqrt{\int_S \frac{1}{4\pi} \Lambda^2 dS} =$

$\sqrt{\frac{I_1}{3}}$, where Λ is the macroscopic stretch in the direction \mathbf{n} of a unit sphere S and I_1 is the first principal invariant of the right Cauchy-Green tensor. Here, \mathbf{n} serves as the continuous directional random variable. Miehe et al. generalized this method by

employing the p -root averaging $\bar{\Lambda} = \left(\int_S \frac{1}{4\pi} \Lambda^p dS \right)^{\frac{1}{p}}$ [7]. Nevertheless, such averaging requires numerical integration over the unit sphere which is prone to numerical error [1, 8]. By considering affine deformation, Wu and van der Giessen obtained

the free energy of an elastomer network as an isotropic averaging of its directional analogy as $\Psi = \int_S \frac{1}{4\pi} \psi \left(\frac{\mathbf{n}}{\Lambda} \right) dS$ [9]. This

approach leads to the development of a family of microsphere models, as extensively reviewed in [10]. Tkachuk and Linder [11] refined the microsphere model by introducing a non-affine stretch vector $\boldsymbol{\lambda}(\mathbf{n})$ into the constrained optimization problem as $\Psi = \min_{\boldsymbol{\lambda}} \int_S \frac{1}{4\pi} \psi(\|\boldsymbol{\lambda}(\mathbf{n})\|) dS$ subject to a particular condition $\int_S \frac{1}{4\pi} \boldsymbol{\lambda}(\mathbf{n}) \otimes \mathbf{n} dS = \frac{1}{3} \mathbf{F}$ for tetrafunctional networks.

Similarly, Govindjee and colleagues [12] extended the non-affine microsphere concept to viscoelastic media by introducing mathematical constraints on the (elastic/viscous) microscopic Hencky strain tensor $\ln \mathbf{u}(\mathbf{n})$ as $\int_S \frac{1}{4\pi} \ln \mathbf{u}(\mathbf{n}) dS = \ln \mathbf{U}$, where

$\ln \mathbf{U}$ represents the corresponding macroscopic counterpart. Verron and Gros postulated a different interpretation of non-affine deformation by employing an equal-force model for polymer molecules with varying chain lengths arranged in series [13]. Accordingly, the non-affine fluctuation arises due to the difference between the number of Kuhn segments in the real and the representative chain. Recently, Britt and Ehret [14] proposed another homogenization scheme, in which the average free energy of fiber network is obtained by utilizing a probability distribution of stretch as $\Psi = \int_{R^+} \rho(\lambda) \psi(\lambda) d\lambda$. In summary,

the emphasis on stretch as the only quantity of interest, coupled with an implicit assumption on isotropic distribution of the random variable, has constrained the applicability of the aforementioned continuous homogenization methods to a particular subset of materials and exclusively to a single deformation mode at large strain. Moreover, the extension of these approaches to contexts beyond their original scope and kinematic measure remains questionable.

In contrast, a statistical homogenization scheme called analytical network-averaging has emerged. It yields explainable invariants of the macroscopic strain tensor, such as average stretch, average area contraction, and average amount of shear [1, 15–19]. The core of such theory is the presence of an orientational distribution function of material directions, such as fibers or polymer chains, as observed via X-ray diffraction [20]. Unlike previous methods, this scheme does not fixate on specific kinematic measures, rendering it applicable across a broad spectrum of soft materials and deformation states when the associated boundary value problem is appropriately formulated. Furthermore, it accommodates deformation history within a generally anisotropic distribution function of material directions, resulting in a unified formulation applicable not only to nonlinear isotropic elasticity but also to anisotropic damage and anisotropic phase transition. Implementation of this methodology to specific soft materials, such as double-network hydrogels and textile reinforcements, facilitates the elucidation of unique properties, including damage cross-effect and irreversible fiber sliding. While the effectiveness of the analytical network-averaging homogenization scheme has been evidenced through various illustrative examples, a thorough exposition of the theory remains elusive, primarily due to the concise nature preferred in conventional scientific articles and the specific

thematic emphasis of individual publications. This review series addresses this gap, starting with an exhaustive theoretical examination of the analytical network-averaging homogenization scheme.

The paper is organized as follows. Section 2 presents the formulations of the analytical network-averaging concept, considering both two-dimensional and three-dimensional scenarios. In contrast to other homogenization schemes, this methodology consistently yields analytical solutions for the homogenized kinematic measures circumventing numerical errors. Implementation of this approach guarantees the achievement of realistic and interpretable stress response functions, accounting for non-affine deformation, material objectivity and material symmetry, as detailed in Sects. 3 and 4. Adoption of the homogenized strain measures to the context of thermodynamics of internal variables furnishes a physical interpretation of the damage cross-effect in double-network hydrogels (Sect. 5). Finally, Sect. 6 discusses a simple example elucidating the application of the homogenization scheme in nonlinear isotropic elasticity of unfilled rubbers.

2 Analytical network-averaging theory

The analytical network-averaging homogenization scheme [1, 15–19] consists of three ingredients. First, it entails the consideration of material direction \mathbf{n} , representing structural element of soft materials such as fibers or polymer chains, as a random variable distributed continuously at the material point. Second, it utilizes a unimodal probability distribution function of the material direction. The concentration parameter of this distribution function quantifies the degree of dispersion of the material direction around a mean axis, which typically corresponds to the alignment direction of chains observed in X-ray diffraction measurements. This probability distribution function captures any alterations in the material microstructure, whether induced by damage or phase transition. Third, the scheme addresses the boundary value problem associated with the RVE of the material microstructure. This boundary value problem yields microscopic kinematic measures of the RVE, which, in turn, indicate the corresponding types of macroscopic strain measures. By means of the unimodal distribution function, the microscopic kinematic measures of the RVE can be analytically derived through statistical averaging of the macroscopic strain measures over the domain of the random variable. Subsequent sections will elaborate on the individual ingredients of our homogenization scheme.

2.1 Unimodal probability distribution function of material direction

In this section, we will introduce two types of distribution function tailored for soft materials distinguished by their solid and shell structures.

2.1.1 Unimodal spherical distribution

The unimodal spherical distribution of material directions is particularly relevant to soft materials characterized by solid-like structures, such as elastomers and biological tissues. Such distribution function can be defined on the basis of the even von Mises-Arnold-Fisher distribution function [15, 21, 22] as

$$\rho(\mathbf{n}) = \hat{\rho}(\theta_i, \zeta_i, \mathbf{M}) = \frac{\zeta_i}{4\pi \sinh(\zeta_i)} \cosh(\zeta_i \cdot \cos \theta_i), \quad (1)$$

where θ_i is the angle between the material direction \mathbf{n} and the mean axis \mathbf{M} . ζ_i denotes the concentration parameter to be discussed later. The vectors \mathbf{n} and \mathbf{M} are normalized to unit magnitude.

In statistics, we are particularly interested in the second moment \mathbf{M} of the distribution function of \mathbf{n} as it provides information about local dispersion of directional data. The second moment of the distribution (1) can be given by [15]

$$\mathbf{M} = \int_0^{2\pi} \int_0^\pi \rho(\mathbf{n}) \mathbf{n} \otimes \mathbf{n} \sin \theta_i d\varphi_i d\theta_i = (1 - w_i) \frac{\mathbf{I}}{3} + w_i \mathbf{M} \otimes \mathbf{M}. \quad (2)$$

Therein, \mathbf{I} denotes the three-dimensional identity tensor, while the volume fraction of oriented material directions w_i can be expressed as [15]

$$w_i = \int_0^{2\pi} \int_0^\pi \hat{\rho}(\theta_i, \varsigma_i, \mathbf{M}) \left(\cos^2 \theta_i \sin \theta_i - \sin^3 \theta_i \cos^2 \varphi_i \right) d\varphi_i d\theta_i = \frac{\varsigma_i^2 - 3 \coth(\varsigma_i) \varsigma_i + 3}{\varsigma_i^2}. \quad (3)$$

The physical interpretation of w_i can be elucidated through asymptotic analysis of Eq. 3. Specifically, in the scenario where $\lim_{\varsigma_i \rightarrow \infty} w_i = 1$, all material directions align toward \mathbf{M} . Conversely, when $\lim_{\varsigma_i \rightarrow 0} w_i = 0$, material directions are uniformly distributed in the unit sphere.

2.1.2 Unimodal circular distribution

The unimodal circular distribution of material directions finds applicability in the analysis of soft materials possessing a shell-like structure, exemplified by textile reinforcements including dry non-crimp fabrics and dry woven fabrics [23]. Such materials are defined by a thickness that is much smaller than their other dimensions. Consequently, the normal stress acting on the mid-surface of the shell can be assumed negligible. Thus, it necessitates the development of a distinct distribution function to address such unique feature.

The unimodal circular distribution function of material direction can be defined as [19]

$$\rho(\mathbf{n}) = \hat{\rho}(\theta_i, \varsigma_i, \mathbf{M}_i) = \frac{\exp(\varsigma_i \min(\theta_i, 2\pi - \theta_i)) + \exp(-\varsigma_i \min(\theta_i, 2\pi - \theta_i) + \pi \varsigma_i)}{4(\exp(\pi \varsigma_i) - 1)}, \quad (4)$$

where $\theta_i = \arccos(\mathbf{n} \cdot \mathbf{M}_i)$ represents the angle between the material direction \mathbf{n} and the mean direction \mathbf{M}_i .

The second moment of the distribution (4) is calculated as [19]

$$\mathbf{M}_i = \int_0^{2\pi} \rho(\mathbf{n}) \mathbf{n} \otimes \mathbf{n} d\theta_i = (1 - w_i) \mathbf{N}_i \otimes \mathbf{N}_i + w_i \mathbf{M}_i \otimes \mathbf{M}_i. \quad (5)$$

Therein, the material direction can be expressed as $\mathbf{n} = \cos \theta_i \mathbf{M}_i + \sin \theta_i \mathbf{N}_i$ and the unit vector \mathbf{N}_i is perpendicular to \mathbf{M}_i . The coefficient w_i can be expressed as follows [19]

$$w_i = \int_0^{2\pi} \hat{\rho}(\theta_i, \varsigma_i, \mathbf{M}_i) \cos^2 \theta_i d\theta_i = \frac{\varsigma_i^2 + 2}{\varsigma_i^2 + 4}. \quad (6)$$

w_i denotes the area fraction of oriented material directions with two asymptotic cases $w_i = \lim_{\varsigma_i \rightarrow \infty} \frac{\varsigma_i^2 + 2}{\varsigma_i^2 + 4} = 1$ for perfectly aligned material directions and $w_i = \lim_{\varsigma_i \rightarrow 0} \frac{\varsigma_i^2 + 2}{\varsigma_i^2 + 4} = \frac{1}{2}$ for isotropically distributed material directions on the unit circle.

2.1.3 Concentration parameter

X-ray diffraction measurements show that the alignment of material directions in soft materials depends on deformation (see, e.g., [20, 24]). To account for such evolution of the distribution function of material directions, we postulated that the concentration parameters of the aforementioned unimodal probability distribution functions (1) and (4) are dependent on the deformation history. Thus, a general formulation of the concentration parameter can be expressed at time t , omitting explicit reference to the material point \mathbf{X} , as follows [15]

$$\varsigma_i(t) = \mathcal{M}_{\tau \in (-\infty, t]} [\mathbf{F}(\tau), \mathbf{E}], \quad (7)$$

where τ denotes a past point in time. Here, the response functional \mathcal{M} maps the history of deformation into the concentration parameter ζ_i , \mathbf{F} represents the deformation gradient and $\mathbf{\Xi}$ denotes an internal variable. ζ_i can be obtained from the inverse function $w_i^{-1}(\zeta_i)$, where $w_i(\zeta_i)$ are given by Eqs. 3 or 6.

Distinct forms of the response functional \mathcal{M} can govern various mechanisms, such as elastically non-affine deformation, damage, or phase transition (Fig. 1). Specific formulations for each scenario will be elucidated in the subsequent part of this series, see also [1, 16, 17, 25].

2.2 Microscopic boundary value problems

The microscopic boundary value problem for the RVE in our homogenization scheme is defined by

$$\text{Div}(\bar{\mathbf{P}}(\bar{\boldsymbol{\alpha}})) = \boldsymbol{\theta}, \quad (8)$$

where $\bar{\mathbf{P}}$ denotes the generalized first Piola-Kirchhoff stress at the micro level and $\bar{\boldsymbol{\alpha}}$ represents the generalized microscopic kinematic measure tensor whose eigenvalues $\bar{\alpha}_k$ correspond to microscopic kinematic measures. Note that the dimensions of $\bar{\mathbf{P}}$, $\bar{\boldsymbol{\alpha}}$ and $\boldsymbol{\theta}$ depend on the required number of microscopic kinematic measures. The constitutive law can be specified through a free energy density function Ψ , the definition of which will be elucidated in Sect. 2.3. Accordingly,

$$\bar{\mathbf{P}} = \frac{\partial \Psi(\bar{\boldsymbol{\alpha}})}{\partial \bar{\boldsymbol{\alpha}}}. \quad (9)$$

Thus, once the microscopic kinematic measures are specified, the microscopic boundary value problem can be solved.

In our homogenization scheme, the microscopic kinematic measures can be defined as the root mean square of the macroscopic kinematic measures

$$\bar{\alpha}_k = \langle \overset{n}{\alpha}_k \rangle_{\text{RMS}} = \left[\int_S \rho(\mathbf{n}) \left(\overset{n}{\alpha}_k \right)^2 dS \right]^{\frac{1}{2}}, \quad (10)$$

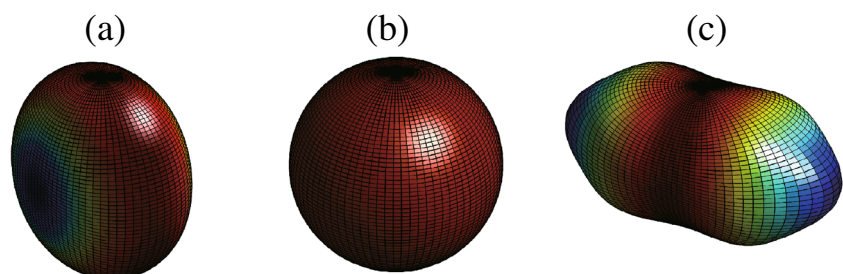
where $\overset{n}{\alpha}_k$ are the corresponding macroscopic kinematic measures.

This principle will be exemplified through two common scenarios encountered in the analysis of soft materials, characterized by solid-like and shell-like structures.

2.2.1 Kinematic measures for macromolecular networks

In macromolecular networks, external forces are applied to the macromolecules via both chain ends and neighboring chains forming topological constraints. Consequently, the RVE of such networks can be conceptualized using a tube model characterized by an end-to-end distance L and a diameter D (Fig. 2). Thus, the microscopic kinematic measures for the RVE of macromolecular networks are tube stretch $\bar{\Lambda} = \frac{l}{L}$ and tube contraction $\bar{\Upsilon} = \frac{d^2}{D^2}$, where l and d are the length and diameter of the tube in the current configuration, respectively. At the macroscale, the corresponding kinematic measures are the change in length $\overset{n}{\Lambda} = \sqrt{\mathbf{C} : \mathbf{n} \otimes \mathbf{n}}$ in the direction \mathbf{n} and the change in area $\overset{n}{\Upsilon} = \sqrt{\text{cof } \mathbf{C} : \mathbf{n} \otimes \mathbf{n}}$ of the cross-section with the normal vector \mathbf{n} , where \mathbf{C} is the right Cauchy-Green tensor, and $\text{cof } \mathbf{C} = \mathbf{C}^{-T} \det \mathbf{C}$ denotes its cofactor.

Fig. 1 Illustration of the spherical distribution function of material directions for examples for: (a) damage, (b) rubber elasticity, and (c) phase transition



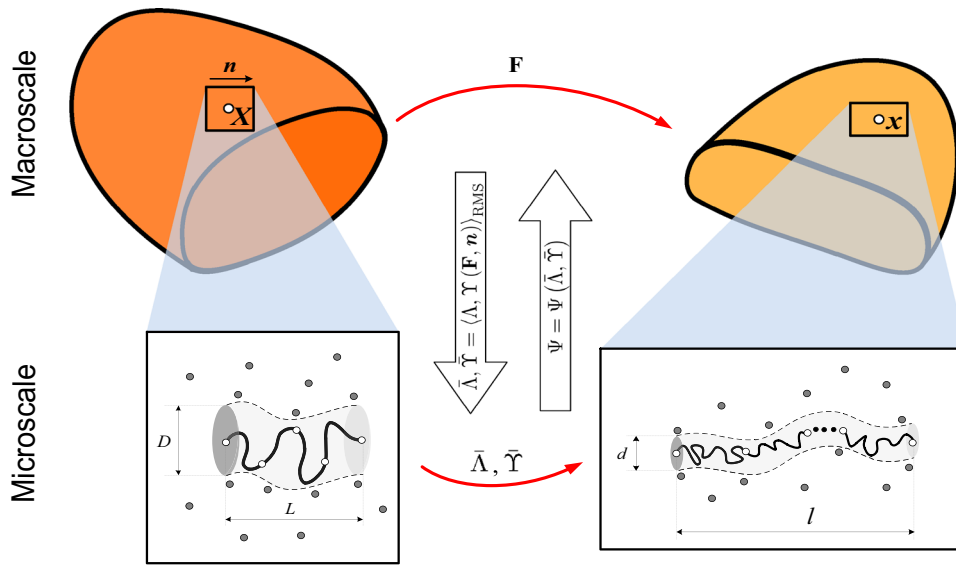


Fig. 2 Homogenization scheme and the RVE for macromolecular networks. The filled circles indicate the cross-sections of adjacent chains

In view of Eqs. 10 and 2, two kinematic measures for macromolecular networks are given by

$$\begin{aligned} \bar{\Lambda} &= \left\langle \frac{n}{\Lambda} \right\rangle_{\text{RMS}} = \left[\mathbf{C} : \int_0^{2\pi} \int_0^\pi \rho(\mathbf{n}) \mathbf{n} \otimes \mathbf{n} \sin \theta_i d\theta_i d\varphi_i \right]^{\frac{1}{2}}, \\ &= [\mathbf{C} : \mathbf{M}]^{\frac{1}{2}} = \left[(1 - w_i) \frac{I_1}{3} + w_i \mathbf{C} : \mathbf{M} \otimes \mathbf{M} \right]^{\frac{1}{2}}, \end{aligned} \tag{11}$$

$$\bar{\Upsilon} = \left\langle \frac{n}{\Upsilon} \right\rangle_{\text{RMS}} = [\text{cof } \mathbf{C} : \mathbf{M}]^{\frac{1}{2}} = \left[(1 - w_i) \frac{I_2}{3} + w_i \text{cof } \mathbf{C} : \mathbf{M} \otimes \mathbf{M} \right]^{\frac{1}{2}}, \tag{12}$$

where I_2 is the second invariant of the right Cauchy-Green tensor. It is easily seen that (11) and (12) represent two invariants of the right Cauchy-Green tensor \mathbf{C} with physical meaning of average stretch and average area contraction.

2.2.2 Kinematic measures for textile reinforcements

For dry textile reinforcements (such as woven fabrics and non-crimp fabrics) characterized by the presence of two yarns, the orientation of fibers within each yarn is described by two independent random variables, denoted as \mathbf{m} and \mathbf{n} . When fibers within a yarn do not align perfectly in a single direction, the dispersion of fibers around the mean direction \mathbf{M}_i in family i is captured by a concentration parameter ς_i ($i = 1, 2$). Consequently, the distribution of fibers in the two families can be written as $\rho(\mathbf{m}) = \hat{\rho}(\mathbf{m}, \varsigma_1, \mathbf{M}_1)$ and $\rho(\mathbf{n}) = \hat{\rho}(\mathbf{n}, \varsigma_2, \mathbf{M}_2)$, where the unimodal distribution function $\hat{\rho}$ is given by Eq. 4. Since the random variables \mathbf{m} and \mathbf{n} are independent of each other, the joint probability distribution of the fiber dispersion can be written as $\rho(\mathbf{m}, \mathbf{n}) = \rho(\mathbf{m})\rho(\mathbf{n})$.

Furthermore, the fibers in a textile reinforcement can be considered inextensible so that the only in-plane deformation mode is shear. Thus, the boundary value problem for an RVE constructed by two material directions \mathbf{m} and \mathbf{n} is defined by the microscopic shear deformation $\bar{\gamma}$ (Fig. 3). At the macroscale, the corresponding kinematic measure is the sine of the shear angle $\Gamma(\mathbf{m}, \mathbf{n}) = \mathbf{C} : \mathbf{m} \otimes \mathbf{n}$.

In view of Eq. 10, the microscopic kinematic measure of the representative volume element for textile reinforcements can be written as

$$\bar{\gamma} = \langle \Gamma(\mathbf{m}, \mathbf{n}) \rangle_{\text{RMS}} = \sqrt{\int_{S_n} \int_{S_m} \rho(\mathbf{m}, \mathbf{n}) (\mathbf{C} : \mathbf{m} \otimes \mathbf{n})^2 dS_m dS_n}, \tag{13}$$

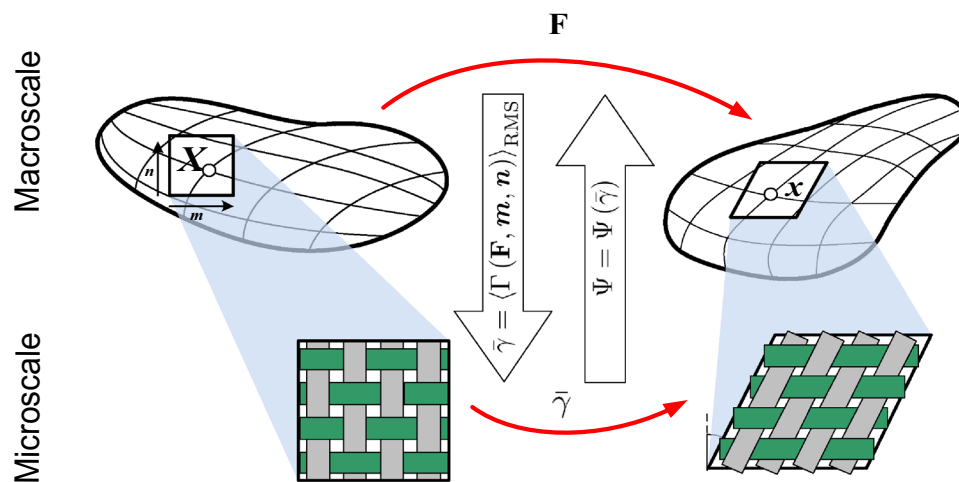


Fig. 3 Homogenization scheme and the RVE for textile reinforcements. The two yarns are in gray and green

where S_m and S_n denote the unit circles of integration.

Leveraging the identity $(\mathbf{C} : \mathbf{m} \otimes \mathbf{n})^2 = \mathbf{C} \odot \mathbf{C} :: \mathbf{m} \otimes \mathbf{n} \odot \mathbf{m} \otimes \mathbf{n} = \mathbf{C} \odot \mathbf{C} :: \mathbf{m} \otimes \mathbf{m} \otimes \mathbf{n} \otimes \mathbf{n}$ and employing (5), the microscopic kinematic measure (13) transforms into

$$\bar{\gamma} = \sqrt{\mathbf{C} \odot \mathbf{C} :: \mathbf{M}_1 \otimes \mathbf{M}_2} \quad (14)$$

where \mathbf{M}_i are the second moment of the unimodal distribution (4) for each fiber family i , and \otimes and \odot are fourth-order tensor products defined by $(\mathbf{A} \otimes \mathbf{B}) : \mathbf{C} = \mathbf{ACB}$ and $(\mathbf{A} \odot \mathbf{B}) : \mathbf{C} = \mathbf{A}(\mathbf{B} : \mathbf{C})$, respectively. The operator $::$ denotes the scalar product of two fourth-order tensors [26], and w_i is the area fraction of fibers in the family i .

The physical significance of the invariant (14) becomes apparent when considering orthotropic continuum media, such as dry woven fabrics. In this case, the microscopic kinematic measure (14) can be expressed as

$$\bar{\gamma} = \sqrt{((1 - w_1)(1 - w_2) + w_1 w_2) |\mathbf{M}_1 \mathbf{C} \mathbf{M}_2|^2 + (1 - w_1) w_2 I_{41}^2 + (1 - w_2) w_1 I_{42}^2}, \quad (15)$$

where $I_{4i} = \mathbf{C} : \mathbf{M}_i \otimes \mathbf{M}_i$ and $i = 1, 2$. This formulation characterizes the microscopic kinematic measure for textile reinforcements as the average amount of shear, defined by the sine of the positive shear angle. Indeed, Eq. 15 represents a weighted averaging of the fiber interaction between two extreme cases: fibers in both families perfectly align in their respective preferred directions, and fibers in one family orient toward the other preferred direction.

2.3 Upscaling transition

In this section, the energetic consistency between two levels of representations is enforced by free energies at these scales. Accordingly, the macroscopic free energy W of the material can be obtained by statistical averaging of the microscopic free energy over the directional data domain S (i.e., unit sphere(s) or unit circle(s) for soft materials with solid-like and shell-like structures, respectively) as

$$W = \int_S \rho(\mathbf{n}) \Psi \left(\frac{\mathbf{n}}{\bar{\alpha}} \right) dS. \quad (16)$$

The microscopic kinematic measures $\frac{\mathbf{n}}{\bar{\alpha}_k}$ are allowed to vary around the macroscopic strain measures $\bar{\alpha}_k^M$ through fluctuating fields f_k [27, 45, 46] as expressed by the following relation

$$\frac{\mathbf{n}}{\bar{\alpha}_k} = f_k \bar{\alpha}_k^M, \quad (k = 1, 2, \dots, m), \quad (17)$$

where m is the number of eigenvalues of the second-order tensor $\bar{\alpha}^n$. Note that m presents the dimension of the homogenization space, not the material body space.

It is further required that micro- and macroscopic kinematic measures take the same values after analytical averaging via Eq. 10 as

$$\left\langle \bar{\alpha}^n \right\rangle_{\text{RMS}} = \bar{\alpha}. \quad (18)$$

According to the principle of minimum potential energy in composite homogenization [7, 28, 29], fluctuation fields represent a solution of the unconstrained optimization

$$\max_{\mathbf{p}} \min_{f_k} \int_S \rho(\mathbf{n}) \Psi \left(\bar{\alpha}^n \right) dS + \mathbf{p} : \left(\left\langle \bar{\alpha}^n \right\rangle_{\text{RMS}} - \bar{\alpha} \right), \quad (19)$$

where \mathbf{p} is the Lagrange multiplier tensor.

The minimization of the Lagrangian results in

$$p_k = - \frac{\partial W}{\partial f_k} \frac{1}{\alpha_k^M}, \quad (k = 1, 2, \dots, m),$$

where p_k are eigenvalues of \mathbf{p} , which should not depend on the spherical coordinates. Thus, a non-affine solution of Eq. 19 is expressed by

$$\bar{\alpha}_k^n = \left\langle \bar{\alpha}_k^n \right\rangle_{\text{RMS}} = \bar{\alpha}_k, \quad (20)$$

independent of the random variable, where the last identity results from Eq. 18. In other words, resolving a single governing equation in the RVE, as outlined in Sect. 2.2, is sufficient for our analytical homogenization scheme.

Furthermore, the macroscopic free energy can be expressed as

$$W = \int_S \rho(\mathbf{n}) \Psi(\bar{\alpha}) dS = \Psi(\bar{\alpha}), \quad (21)$$

which results in the aforementioned microscopic constitutive law (9).

3 Non-affine deformation

In contrast to other continuous homogenization methods, the analytical network-averaging does not fixate on specific kinematic measures, rendering it applicable across a broad spectrum of soft materials and deformation states. This section analyzes the influence of the concentration parameter on the non-affine deformation in multiple contexts, including stretch and area contraction within macromolecular networks, and shear due to fiber sliding in textile reinforcements.

To this end, the average stretch (11) and the average area contraction (12) under uniaxial tension are plotted at different values of the concentration parameter (Fig. 4a, b). Furthermore, by considering mechanically equivalent and inextensible fibers (i.e., $w_1 = w_2$ and $I_{41} = I_{42} = 1$), the average amount of shear (i.e., average sine of the positive shear angle) (15) can be depicted across various values of ζ_i (Fig. 4c).

It can be seen that in all scenarios, affine deformation only occurs at $\zeta_i = \infty$, signifying perfect alignment of material directions. Of particular interest is the microscopic amount of shear $\bar{\gamma}$ at the reference configuration when ζ_i takes a positive but finite value. This non-zero amount of shear at the reference state is attributed to the fiber dispersion. Moreover, in case of isotropic fiber distribution, represented by $\zeta_i = 0$, the mathematically expected positive shear angle is $\frac{\pi}{4}$, resulting in

$\bar{\gamma}(\mathbf{C} = \mathbf{I}) = \frac{1}{\sqrt{2}}$. Note that such a rigorous interpretation of non-affine deformation is, to the best of our knowledge, absent in other continuous homogenization schemes.

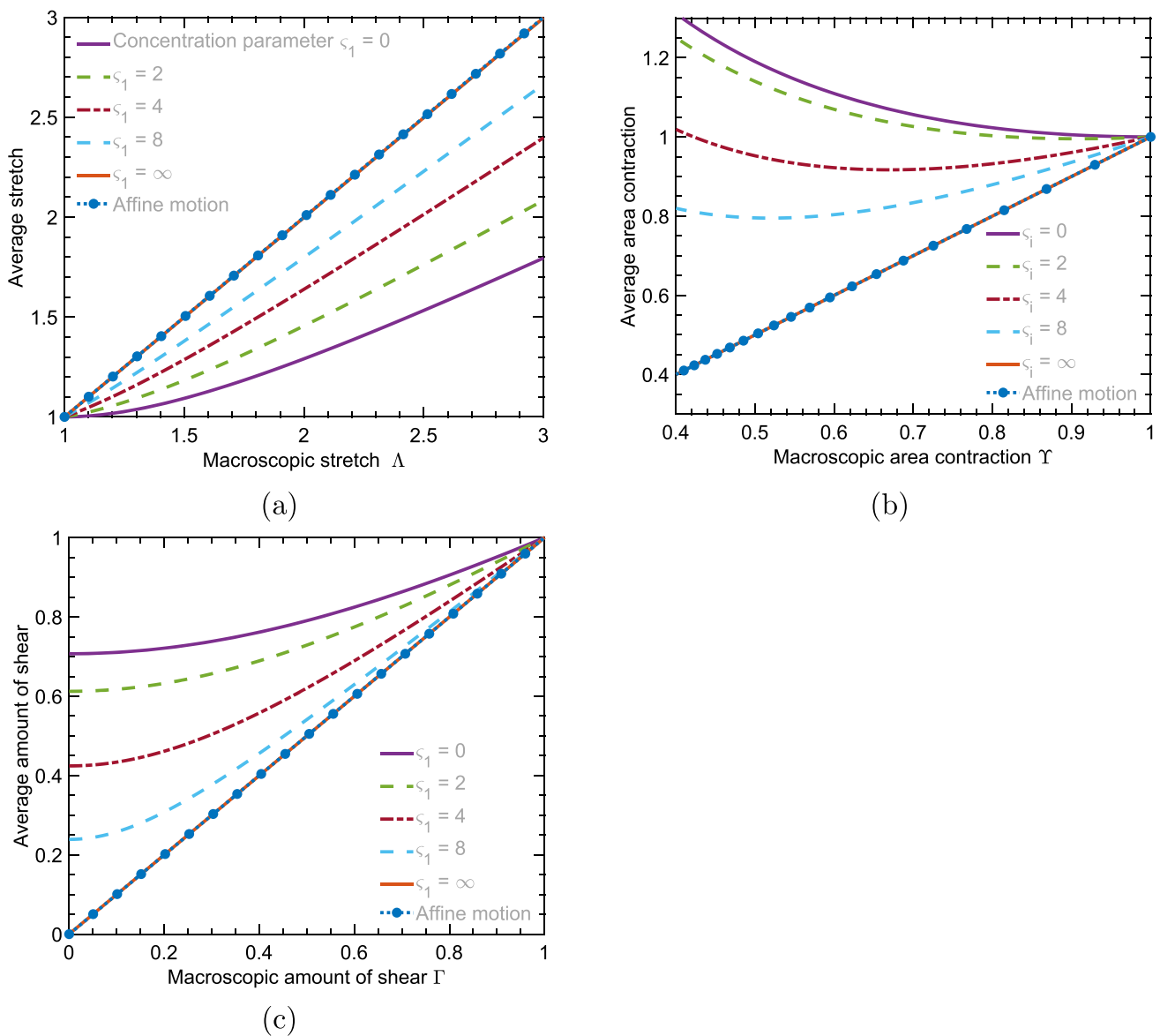


Fig. 4 (a) Microscopic stretch and (b) microscopic area contraction under uniaxial tension; (c) microscopic amount of shear at different values of the concentration parameter

4 Material objectivity and material symmetry

In accordance with Noll's seminal work [30], stress response functions must adhere to certain constitutive principles to ensure their reliability for data analysis. These include the principle of material objectivity (invariance under observer transformations) and the concept of material symmetry (invariance under orthogonal transformation of the reference configuration within the symmetry group \mathbf{G}^0). It is easily seen that all proposed kinematic measures (11), (12) and (15) are defined in terms of \mathbf{C} which is invariant under observer transformations, therefore stress response functions expressed in terms of those invariants automatically fulfil the principle of material objectivity.

Soft materials' constitutive formulations defined on the basis of our homogenization scheme are characterized by the following symmetry group

$$\mathbf{G}^0 = \left\{ \mathbf{Q} \in \text{Orth} \mid \mathbf{Q} \mathbf{M}_i \otimes \mathbf{M}_i \mathbf{Q}^T = \mathbf{M}_i \otimes \mathbf{M}_i \right\},$$

where $i = 1, 2, \dots, n$ with n representing the number of mean directions utilized in the homogenization scheme and **Orth** is the three-dimensional orthogonal tensor space.

The microscopic kinematic measures obtained from the analytical network-averaging (11), (12) and (15) guarantee a priori that rotations and reflections determined by orthogonal tensors among the symmetry group \mathbf{G}^0 do not affect the response function of the constitutive formulations. Indeed, it can be shown that

$$\begin{aligned}\bar{\Lambda}(\mathbf{QCQ}^T, \mathbf{QM}_i \otimes \mathbf{M}_i \mathbf{Q}^T) &= \bar{\Lambda}(\mathbf{C}, \mathbf{M}_i \otimes \mathbf{M}_i), \\ \bar{\Upsilon}(\mathbf{QCQ}^T, \mathbf{QM}_i \otimes \mathbf{M}_i \mathbf{Q}^T) &= \bar{\Upsilon}(\mathbf{C}, \mathbf{M}_i \otimes \mathbf{M}_i), \\ \bar{\gamma}(\mathbf{QCQ}^T, \mathbf{QM}_1 \otimes \mathbf{M}_1 \mathbf{Q}^T, \mathbf{QM}_2 \otimes \mathbf{M}_2 \mathbf{Q}^T) &= \bar{\gamma}(\mathbf{C}, \mathbf{M}_1 \otimes \mathbf{M}_1, \mathbf{M}_2 \otimes \mathbf{M}_2) \quad \forall \mathbf{Q} \in \mathbf{G}^0.\end{aligned}$$

In conclusion, stress response functions (21) inherently adhere to the material objectivity and material symmetry principles.

5 Thermodynamics of internal variables

Constitutive theories concerning macromolecular networks often employ maximal principal stretches acquired during deformation history as internal variables [31]. It is now widely accepted that such internal variables capture independent damage mechanisms across different principal directions of deformation. In particular, such anisotropic damage is very pronounced in filled elastomers [15, 32]. Nevertheless, in materials involving multiple networks, such as double-network hydrogels [33], these mechanisms are not present due to the interpenetration of the networks. Recent multi-axial experimental findings [34] have revealed a damage cross-effect in double-network hydrogels, characterized by the simultaneous influence of damage history in one direction on the damage in other directions. This section illustrates how a straightforward implementation of our microscopic kinematic measures within a thermodynamical framework of internal variables provides a physical interpretation of the damage cross-effect in double-network hydrogels.

To this end, let the maximal microstretch $\bar{\Lambda}_i^{\max}$ previously reached in the deformation history of double-network hydrogels be defined by [18]

$$\bar{\Lambda}_i^{\max} = \max_{\tau \in (-\infty, t]} \bar{\Lambda}_i(\tau), \quad (22)$$

where $i = 1, 2, 3$ specifies the index of the principal direction of the right Cauchy-Green tensor, while the microscopic stretch $\bar{\Lambda}_i$ is defined by Eq. 11. Thus, $\bar{\Lambda}_i^{\max}$ serve as internal variables whose evolution law results from the principle of maximum damage dissipation [15, 25, 35].

For illustrative purposes, one may consider the following directional damage function [18]

$$D_i = 1 - \Phi_0 \exp\left(\frac{\bar{\alpha}}{4\pi} \left[\bar{n} \sin \frac{2\pi \bar{\Lambda}_i^{\max} \bar{L}}{\bar{n}} - 2\pi \bar{\Lambda}_i^{\max} \bar{L} \right]\right), \quad i = 1, 2, 3, \quad (23)$$

where $\Phi_0 = \exp\left(\frac{\bar{\alpha}}{4\pi} \left[2\pi \bar{L} - \bar{n} \sin \frac{2\pi \bar{L}}{\bar{n}} \right]\right)$ is the normalization factor. $\bar{\alpha}$, \bar{n} and \bar{L} denote here positive material parameters whose physical meaning can be found in [18].

The damage cross-effect can be understood by analyzing the evolution of directional damage D_i under a pure shear experiment with stretch ratio up to 2.5 (Fig. 5). Note that damage occurs in the second direction (Fig. 5b — top), despite being constrained (Fig. 5a). Conversely, in models based on maximal principal stretches, no damage happens in the second (unstretched) direction (Fig. 5b — bottom). In the context of double-network hydrogels, our homogenization scheme captures such damage cross-effect through the volume fraction of the first network, $w_1 = 0.35$, which signifies the degree of interpenetration between the two networks. In an extreme scenario of a material with only a single network ($w_1 = 1$), the damage mechanism exhibits independent behavior across different directions, a trend consistently supported by experimental observations [32].

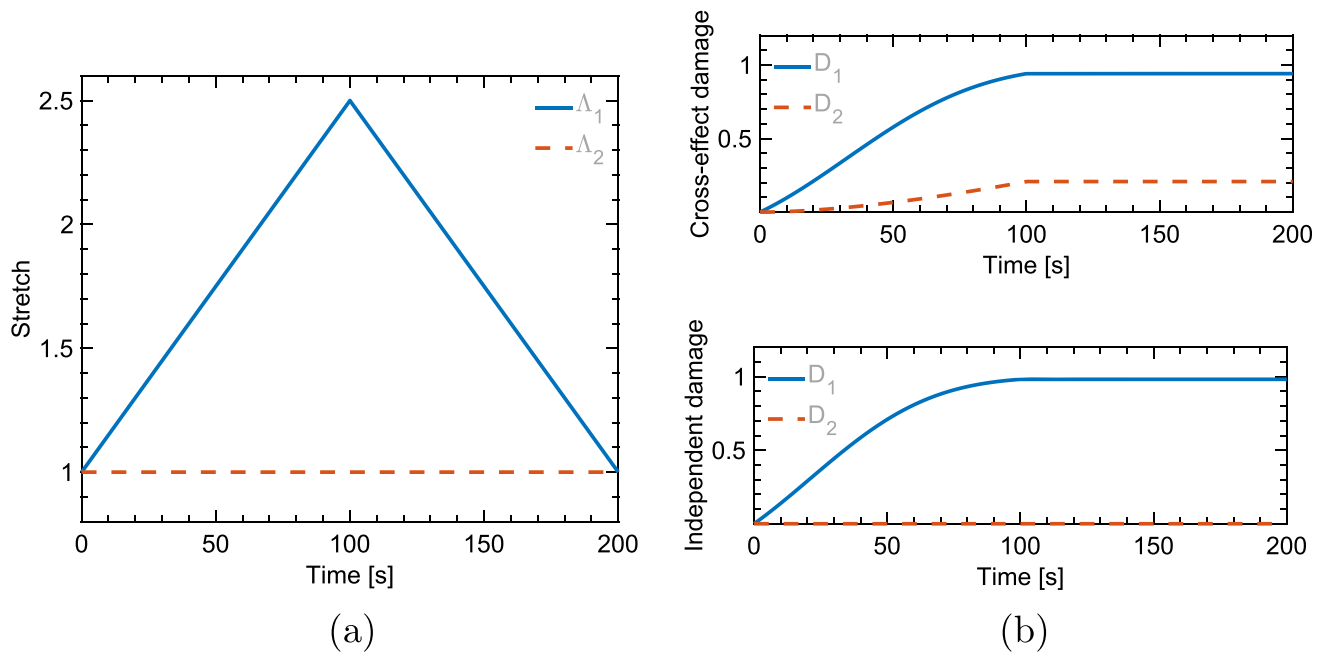


Fig. 5 Difference between damage cross-effect and independent damage mechanisms: (a) deformation history, the sample is subject to a cycle of pure shear; (b) top: damage cross-effect in models based on our microscopic kinematic measure with $w_i = 0.35$ ($\bar{\alpha} = 20$, $\bar{n} = 15$ and $\bar{L} = 1$); (b) bottom: independent damage in models using maximal principal stretches

6 Isotropic application

This section presents a simple example elucidating the application of the analytical network-averaging concept to model unfilled rubbers.

6.1 Microscopic kinematic measures

For an isotropic solid-like material, the directional distribution function takes the form (1) with concentration parameter $\zeta_i = 0$, which results in (Fig. 1b)

$$\rho(\mathbf{n}) = \frac{1}{4\pi}. \quad (24)$$

According to Section 2.2.1, the RVE of the rubber network is a tube with two kinematic measures: microscopic stretch $\bar{\Lambda}$ and microscopic area contraction $\bar{\Upsilon}$. In view of Eqs. 3, 11 and 12, these microscopic kinematic measures are given by

$$\bar{\Lambda} = \sqrt{\frac{I_1}{3}}, \quad (25)$$

$$\bar{\Upsilon} = \sqrt{\frac{I_2}{3}}. \quad (26)$$

It can be seen that the microscopic stretch in this instance coincides with the formulations proposed by Beatty [6], the 4-chain model [36] and the 8-chain model [37]. Nevertheless, our model diverges from theirs due to a distinct choice of the RVE, which incorporates an additional pivotal kinematic measure $\bar{\Upsilon}$.

6.2 Constitutive formulation

The free energy of the rubber network can be postulated as [1]

$$\Psi = \mu_c n \ln \frac{\sin \frac{\pi}{\sqrt{n}} \cdot \bar{\Lambda}}{\sin \left(\frac{\pi}{\sqrt{n}} \bar{\Lambda} \right)} + \mu_t [\bar{\Upsilon} - 1]. \quad (27)$$

where μ_c is the phantom shear modulus, n is the average number of chain segments in the representative tube, and μ_t is the topological shear modulus. In (27), a non-Gaussian free energy, as proposed by Khiêm and Itskov [1], is used instead of the classical inverse-Langevin based strain energy. This is motivated by two key factors: (1) such non-Gaussian free energy derives from a closed-form representation of the non-Gaussian distribution [38], and (2) it ensures quadratic convergence in finite element computations [1].

By regarding unfilled rubber as incompressible, the principal nominal stress can be formulated as

$$P_i = \frac{\mu_c}{3} \left[\frac{n}{\bar{\Lambda}} - \pi \sqrt{n} \cot \frac{\pi \bar{\Lambda}}{\sqrt{n}} \right] \frac{\Lambda_i}{\bar{\Lambda}} + \frac{\mu_t}{3} \frac{\Lambda_i}{\bar{\Upsilon}} \left[\Lambda_j^2 + \Lambda_k^2 \right] - \frac{p_c}{\Lambda_i}, \quad (28)$$

where $i \neq j \neq k \neq i = 1, 2, 3$ and p_c is a Lagrange multiplier resulting from the incompressibility constraint.

6.3 Results

In this section, the performance of the proposed model is validated by comparison with various sets of experimental data from [39–41] and unfilled silicone rubbers [42].

First, the material constants μ_c , n , and μ_t are found (Table 1) by training (27) with experimental data by Treloar on uniaxial tension, pure shear and equibiaxial tension of vulcanized rubbers containing 8phr sulfur [39]. To emphasize the significance of selecting an appropriate RVE for the homogenized constitutive model (Sect. 2.2), the predictive capability of the 8-chain model [37] is demonstrated following its training using the identical dataset. Note that the 8-chain model demonstrates limitations in its performance (Fig. 6b), attributable to an improper choice of microscopic kinematic measures, which solely relies on I_1 . In contrast, the Treloar data can be perfectly fitted by our model (Fig. 6a).

Next, we tested our model on a series of biaxial tension data [40], employing the same set of material parameters.

The rubber samples in both experiments [40] and [39] were reported to have similar chemical composition and mechanical response [43]. The biaxial tension experiments were conducted under various fixed values of stretch Λ_1 , with concurrent adjustments to the stretch Λ_2 in the orthogonal direction, transitioning from uniaxial tension to equibiaxial tension. One observes relatively good agreement between predictions of the model (27) with testing data (Fig. 7). Note that the present model exhibits a slight underperformance in these tests when compared to the original model by Khiêm and Itskov [1], which is likely due to a simpler stress hypothesis. Interested readers are directed to [15] for a comprehensive exploration of the underlying physics governing the stress hypothesis.

Second, the model is evaluated in comparison to experimental data by Yeoh and Flaming [41]. This dataset comprises a series of tension, compression and simple shear experiments performed on vulcanized natural rubbers differing solely in amounts of curatives (sulfur and accelerator): 0.5 (A), 1.0 (B), 1.5 (C) and 2.0 phr (D). Thus, it is anticipated that the phantom shear modulus will be proportional to the amount of sulfur and accelerator present. Furthermore, the number of chain segments in the model (27) can be directly derived from the macro-stretch at failure $\Lambda_{rupture}$ (under uniaxial tension) as a result of the chain extensibility limit [1]. Accordingly,

$$n = \frac{\Lambda_{rupture}^2}{3} + \frac{2}{3\Lambda_{rupture}}. \quad (29)$$

Therein, the macro-stretches at rupture $\Lambda_{rupture}$ were determined according to the ASTM D412 standard [41].

Table 1 Model parameters for Treloar's data

μ_c [MPa]	n	μ_t [MPa]
0.2367	24.9591	0.2020

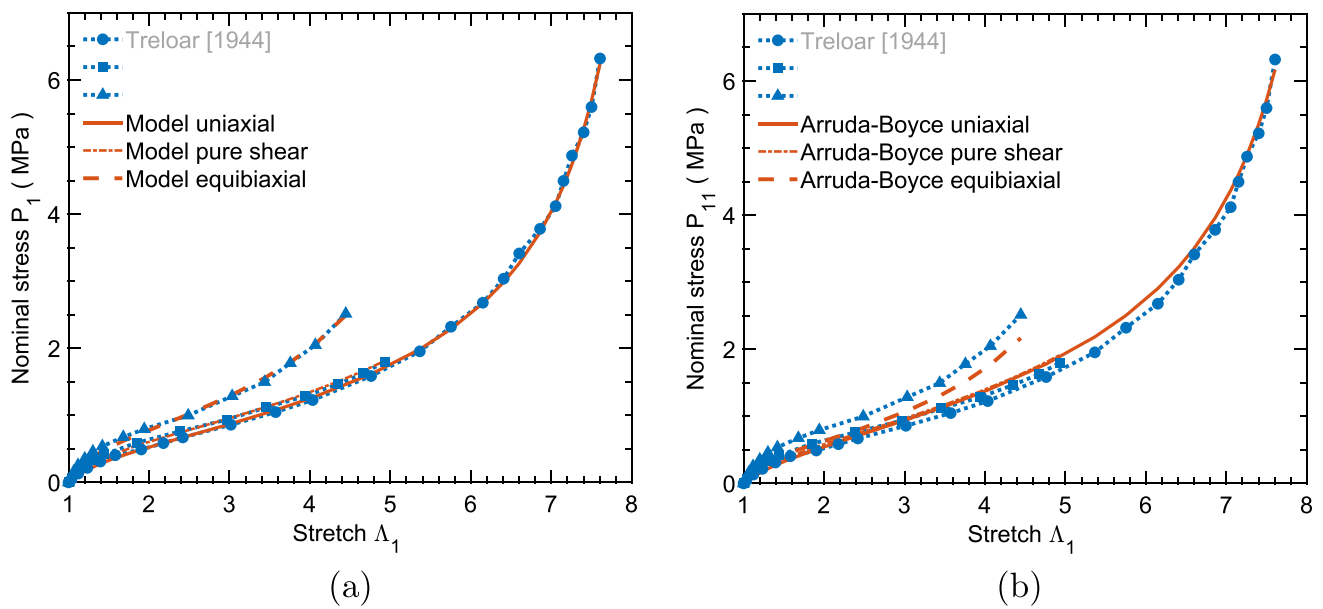


Fig. 6 Predictions of (a) the model (27) and (b) the 8-chain model versus Treloar's data [39]

In order to verify this concept, two material constants μ_c and μ_t of the model are found by training with the experimental data from sample D (see Fig. 8). Subsequently, to predict the behavior of samples A, B, and C, the phantom shear moduli are further considered linearly dependent on the amount of curatives as follows

$$\mu_{c(i)} = \mu_{cD}\varphi(i), \quad (30)$$

where $\varphi(i) = \frac{N_{c0(i)}}{N_{c0D}}$ denotes the ratio between curative contents, and $i = A, B, C$. Furthermore, recent molecular dynamics simulation demonstrated that the topological shear modulus remains constants for cross-linked networks with low network density [44], so that $\mu_{t(i)} = \mu_{tD} = 0.22$. The so-obtained values of material constants are given in Table 2.

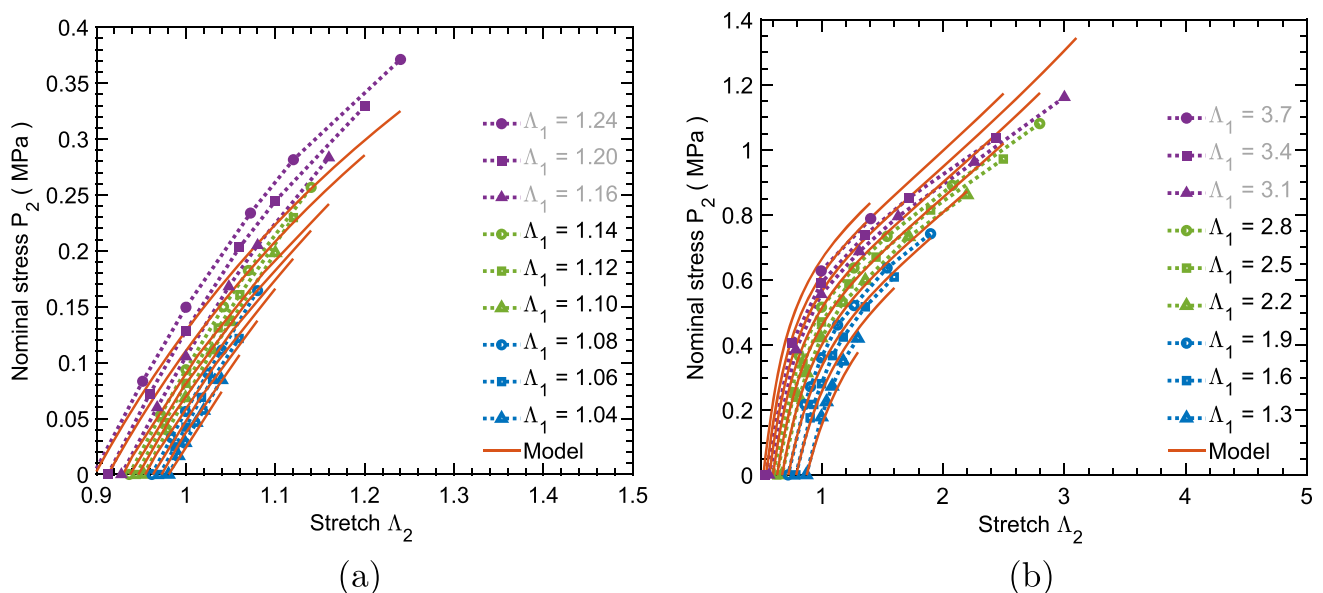


Fig. 7 Testing of the model (27) on a series of biaxial tensions by [40]: (a) at small values of Λ_1 , and (b) at large values of Λ_1 . Material constants used in this calibration are given in Table 1

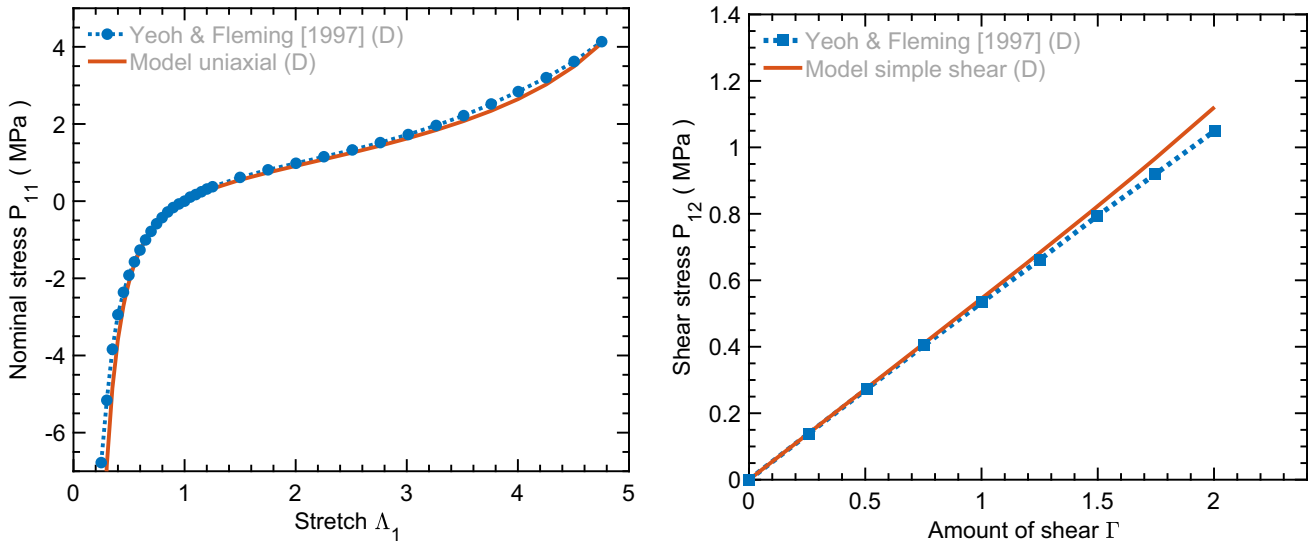


Fig. 8 Training of the proposed model versus stress-strain responses of sample (D) from the experiments by [41]. Fitted parameters: $\mu_c = 0.4082[\text{MPa}]$ and $\mu_t = 0.220[\text{MPa}]$ (cf. [1])

Table 2 Model parameters for Yeoh’s data

Sample	$\mu_c[\text{MPa}]$	n	$\mu_t[\text{MPa}]$	$\Lambda_{rupture}^{ASTM}$
D 2.0phr	<i>0.4082</i>	12.9209	<i>0.2200</i>	6.2
C 1.5	0.3062	15.5114	0.2200	6.8
B 1.0	0.2041	20.8877	0.2200	7.9
A 0.5	0.1021	21.9523	0.2200	8.1

Fitted parameters are italicized

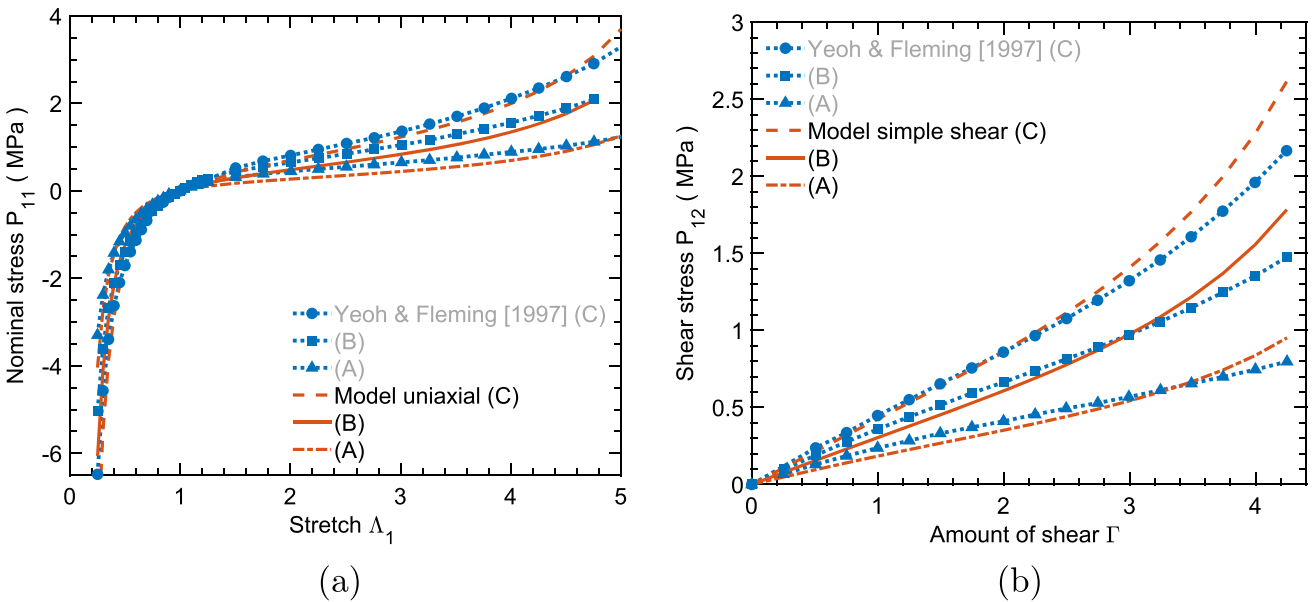


Fig. 9 Testing of the proposed model versus stress-strain responses of samples (A), (B) and (C) versus experimental data by [41]: (a) uniaxial tension, and (b) simple shear

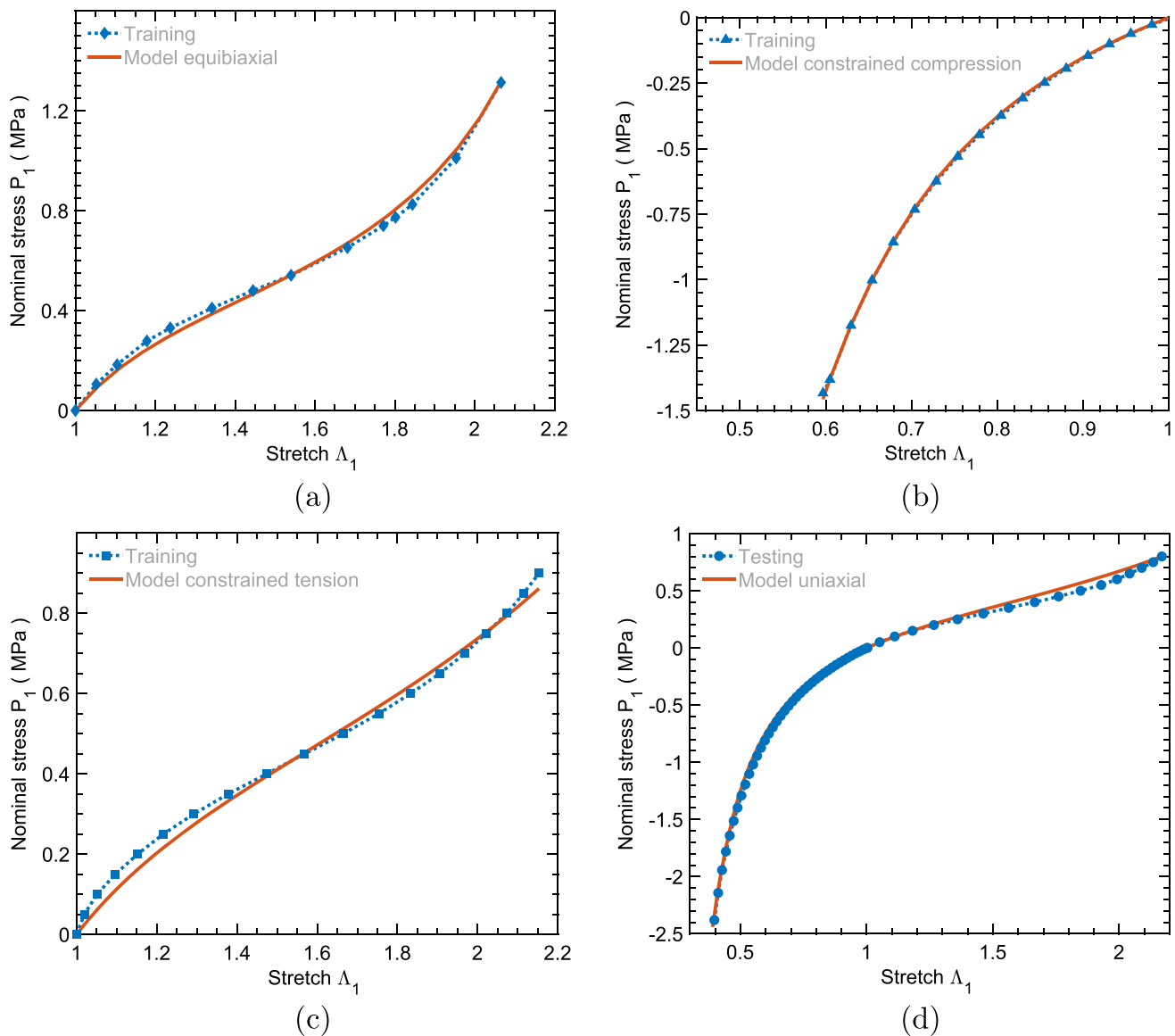


Fig. 10 Evaluation of the model prediction with the experimental data [42] in training: (a) equibiaxial tension, (b) constrained compression, (c) constrained tension, and testing: (d) uniaxial tension and compression

Despite using only two fitting parameters, relatively good agreement with experimental results can be observed when testing with samples A, B, and C (see Fig. 9). By means of Eqs. 29 and 30, the model demonstrates the capability to forecast the mechanical response of the same rubber compound across various network densities using only one set of fitting parameters. Slight discrepancy between the model prediction and the experimental data at large strain could be due to chain alignment resulting from strain-induced crystallization in natural rubbers (see Eq. 3 and further details in [17]), a factor not accounted for within (27).

Finally, the model is trained with experimental data by Meunier et al. [42] encompassing constrained compression and tension (pure shear), and equibiaxial tension of an unfilled silicone rubber (see Fig. 10a–c). The resultant material parameters are given in Table 3. It is worth mentioning that silicone rubber, containing Si atoms in its backbone, classifies as an inorganic

Table 3 Model parameters for Meunier et al.'s data

μ_c [MPa]	n	μ_t [MPa]
0.2438	4.1357	0.0012

polymer. Consequently, the average number of chain segments for this rubber is significantly lower than that of organic polymers (cf. Table 1).

Furthermore, predictive performance of the model, evaluated against testing data from tensile and compressive experiments on the same rubber as depicted in Fig. 10d, demonstrates its generalization capacity.

7 Conclusion

In this paper, we presented a comprehensive review of the theoretical foundation of the analytical network-averaging homogenization framework. It highlighted three fundamental constituents of our continuous homogenization approach: the directional random variable, its generally anisotropic distribution function, and the boundary value problem associated with the RVE of the material microstructure. We assert that validation of these constituents, whether through experimental or theoretical domain expertise, ensures the applicability of the proposed homogenization scheme and yields stress response functions that are both interpretable and physically meaningful. By a priori guaranteeing non-affine deformation, material objectivity, and material symmetry, our framework enhances its utility in diverse soft materials characterized by both solid-like and shell-like behavior. Furthermore, by extending the theory to encompass the thermodynamics of internal variables, we facilitated the interpretation of phenomena such as the newly observed damage cross-effect, a distinctive feature of modern soft materials like multiple-network hydrogels. To further demonstrate the interpretability of the constitutive formulation derived from our homogenization scheme, we presented an illustrative modeling example focusing on isotropic nonlinear elasticity. This example was applied to multi-axial experimental data obtained from a diverse range of unfilled rubbers. It is important to emphasize that regardless of the efficacy or limitations observed in the evaluation of the model, such outcomes are always explainable using our homogenization scheme. We contend that such interpretability, rather than fitting capability, is paramount in the age of data science, as it is what humans truly learn from data.

Funding Open Access funding enabled and organized by Projekt DEAL.

Availability of data and materials The datasets produced in this study can be obtained from the corresponding author upon reasonable request.

Declarations

Conflict of interest The authors declare no competing interests.

Open Access This article is licensed under a Creative Commons Attribution 4.0 International License, which permits use, sharing, adaptation, distribution and reproduction in any medium or format, as long as you give appropriate credit to the original author(s) and the source, provide a link to the Creative Commons licence, and indicate if changes were made. The images or other third party material in this article are included in the article's Creative Commons licence, unless indicated otherwise in a credit line to the material. If material is not included in the article's Creative Commons licence and your intended use is not permitted by statutory regulation or exceeds the permitted use, you will need to obtain permission directly from the copyright holder. To view a copy of this licence, visit <http://creativecommons.org/licenses/by/4.0/>.

References

1. Khiêm, V.N., Itskov, M.: Analytical network-averaging of the tube model. *J. Mech. Phys. Solids* **95**, 254–269 (2016). <https://doi.org/10.1016/j.jmps.2016.05.030>
2. Kouznetsova, V., Brekelmans, W.A.M., Baaijens, F.P.T.: An approach to micro-macro modeling of heterogeneous materials. *Comput. Mech.* **27**(1), 37–48 (2001)
3. Blanco, P.J., Sánchez, P.J., Souza Neto, E.A., Feijóo, R.A.: Variational foundations and generalized unified theory of rve-based multiscale models. *Arch. Comput. Methods Eng.* **23**, 191–253 (2016)
4. Hill, R.: Elastic properties of reinforced solids: some theoretical principles. *J. Mech. Phys. Solids* **11**(5), 357–372 (1963)
5. Mandel, J.: *Plasticité classique et viscoplasticité* (CISM, Udine, 1971). Springer (1972)
6. Beatty, M.F.: An average-stretch full-network model for rubber elasticity. *J. Elast.* **70**, 65–86 (2003). https://doi.org/10.1007/1-4020-2308-1_7
7. Miehe, C., Göktepe, S., Lulei, F.: A micro-macro approach to rubber-like materials - Part I: The non-affine micro-sphere model of rubber elasticity. *J. Mech. Phys. Solids* **52**(11), 2617–2660 (2004). <https://doi.org/10.1016/j.jmps.2004.03.011>
8. Veron, E.: Questioning numerical integration methods for microsphere (and microplane) constitutive equations. *Mech. Mater.* **89**, 216–228 (2015). <https://doi.org/10.1016/j.mechmat.2015.06.013>
9. Wu, P.D., Giessen, E.: On improved network models for rubber elasticity and their applications to orientation hardening in glassy polymers. *J. Mech. Phys. Solids* **41**(3), 427–456 (1993). [https://doi.org/10.1016/0022-5096\(93\)90043-F](https://doi.org/10.1016/0022-5096(93)90043-F)

10. Dargazany, R., Khiêm, V.N., Itskov, M.: A generalized network decomposition model for the quasi-static inelastic behavior of filled elastomers. *Int. J. Plast.* **63**, 94–109 (2014). <https://doi.org/10.1016/j.ijplas.2013.12.004>
11. Tkachuk, M., Linder, C.: The maximal advance path constraint for the homogenization of materials with random network microstructure. *Phil. Mag.* **92**(22), 2779–2808 (2012)
12. Govindjee, S., Zoller, M.J., Hackl, K.: A fully-relaxed variationally-consistent framework for inelastic micro-sphere models: finite viscoelasticity. *J. Mech. Phys. Solids* **127**, 1–19 (2019). <https://doi.org/10.1016/j.jmps.2019.02.014>
13. Verron, E., Gros, A.: An equal force theory for network models of soft materials with arbitrary molecular weight distribution. *J. Mech. Phys. Solids* **106**, 176–190 (2017). <https://doi.org/10.1016/j.jmps.2017.05.018>
14. Britt, B.R., Ehret, A.E.: Constitutive modelling of fibre networks with stretch distributions. Part I: Theory and illustration. *J. Mech. Phys. Solids* **167**, 104960 (2022). <https://doi.org/10.1016/j.jmps.2022.104960>
15. Khiêm, V.N., Itskov, M.: An averaging based tube model for deformation induced anisotropic stress softening of filled elastomers. *Int. J. Plast.* **90**, 96–115 (2017). <https://doi.org/10.1016/j.ijplas.2016.12.007>
16. Khiêm, V.N., Itskov, M.: Analytical network-averaging of the tube model: mechanically induced chemiluminescence in elastomers. *Int. J. Plast.* **102**, 1–15 (2018). <https://doi.org/10.1016/j.ijplas.2017.11.001>
17. Khiêm, V.N., Itskov, M.: Analytical network-averaging of the tube model: strain-induced crystallization in natural rubber. *J. Mech. Phys. Solids* **116**, 350–369 (2018). <https://doi.org/10.1016/j.jmps.2018.04.003>
18. Khiêm, V.N., Mai, T.-T., Urayama, K., Gong, J.P., Itskov, M.: A multiaxial theory of double network hydrogels. *Macromolecules* **52**(15), 5937–5947 (2019). <https://doi.org/10.1021/acs.macromol.9b01044>
19. Khiêm, V.N., Jabareen, M., Poudel, R., Tang, X., Itskov, M.: Modeling of textile composite using analytical network averaging and gradient damage approach. Preprint submitted to *Journal of the Mechanics and Physics of Solids* (2024) <https://doi.org/10.2139/ssrn.4737597>
20. Toki, S., Sics, I., Ran, S., Liu, L., Hsiao, B.S., Murakami, S.O., Senoo, K., Kohjiya, S.: New insights into structural development in natural rubber during uniaxial deformation by in situ synchrotron X-ray diffraction. *Macromolecules* **35**(17), 6578–6584 (2002). <https://doi.org/10.1021/ma0205921>
21. Fisher, R.: Dispersion on a sphere. *Proc. R. Soc. Lond. Ser. A Math. Phys. Sci.* **217**(1130), 295–305 (1953)
22. Mourzenko, V.V., Thovert, J.F., Adler, P.M.: Permeability of isotropic and anisotropic fracture networks, from the percolation threshold to very large densities. *Phys. Rev. E Stat. Nonlin. Soft Matter Phys.* **84**(3), 1–20 (2011). <https://doi.org/10.1103/PhysRevE.84.036307>
23. Khiêm, V.N., Krieger, H., Itskov, M., Gries, T., Stapleton, S.: An averaging based hyperelastic modeling and experimental analysis of non-crimp fabrics. *Int. J. Solids Struct.* **154**, 43–54 (2018). <https://doi.org/10.1016/j.ijsolstr.2016.12.018>
24. Beurrot-Borgarino, S.: Crystallisation sous contrainte du caoutchouc naturel en fatigue et sous sollicitation multiaxiale. PhD thesis, École centrale de Nantes (ECN) (2012)
25. Khiêm, V.N., Le Cam, J.-B., Charlès, S., Itskov, M.: Thermodynamics of strain-induced crystallization in filled natural rubber under uni- and biaxial loadings. Part II: Physically-based constitutive theory. *J. Mech. Phys. Solids* **159**, 104712 (2022). <https://doi.org/10.1016/j.jmps.2021.104712>
26. Itskov, M.: *Tensor Algebra and Tensor Analysis for Engineers*, 3rd edn. Springer, Berlin Heidelberg (2012)
27. Bertram, A., Böhlke, T., Kraska, M.: Numerical simulation of deformation induced anisotropy of polycrystals. *Comput. Mater. Sci.* **9**(1–2), 158–167 (1997)
28. Castaneda, P.P., Suquet, P.: *Nonlinear Composites*. *Adv. Appl. Mech.* **34**(998), 171–302 (1998)
29. Khiêm, V.N.: *Analytical Network Averaging Concept for Physically-based Modeling of Rubber-like Materials*. PhD Thesis No.6, Department of Continuum Mechanics. RWTH Aachen University, Aachen (2018)
30. Noll, W.: A mathematical theory of the mechanical behavior of continuous media. *Arch. Ration. Mech. Anal.* **2**(1), 197–226 (1958). <https://doi.org/10.1007/BF00277929>
31. Govindjee, S., Simo, J.: A micro-mechanically based continuum damage model for carbon black-filled rubbers incorporating Mullins' effect. *J. Mech. Phys. Solids* **39**, 87–112 (1991). [https://doi.org/10.1016/0022-5096\(91\)90032-J](https://doi.org/10.1016/0022-5096(91)90032-J)
32. Mai, T.T., Morishita, Y., Urayama, K.: Induced anisotropy by Mullins effect in filled elastomers subjected to stretching with various geometries. *Polymer* **126**, 29–39 (2017). <https://doi.org/10.1016/j.polymer.2017.08.012>
33. Gong, J.P., Katsuyama, Y., Kurokawa, T., Osada, Y.: Double-network hydrogels with extremely high mechanical strength. *Adv. Mater.* **15**(14), 1155–1158 (2003). <https://doi.org/10.1002/adma.200304907>
34. Mai, T.-T., Matsuda, T., Nakajima, T., Gong, J.P., Urayama, K.: Distinctive characteristics of internal fracture in tough double network hydrogels revealed by various modes of stretching. *Macromolecules* **51**(14), 5245–5257 (2018). <https://doi.org/10.1021/acs.macromol.8b01033>
35. Hill, R.: A theory of the yielding and plastic flow of anisotropic metals. *Proc. R. Soc. Lond. Ser. A Math. Phys. Sci.* **193**(1033), 281–297 (1948)
36. Wang, M.C., Guth, E.: Statistical theory of networks of non-gaussian flexible chains. *J. Chem. Phys.* **20**, 1144–1157 (1952). <https://doi.org/10.1063/1.1700682>
37. Arruda, E.M., Boyce, M.C.: A three-dimensional constitutive model for the large stretch behavior of rubber elastic materials. *J. Mech. Phys. Solids* **41**(2), 389–412 (1993). [https://doi.org/10.1016/0022-5096\(93\)90013-6](https://doi.org/10.1016/0022-5096(93)90013-6)
38. Lord Rayleigh, J.W.S.: On the problem of random vibrations, and of random flights in one, two, or three dimensions. *Phil. Mag.* **37**(6), 321–347 (1919). <https://doi.org/10.1080/14786440408635894>
39. Treloar, L.R.G.: Stress-strain data for vulcanised rubber under various types of deformation. *Trans. Faraday Soc.* **40**, 59–70 (1944)
40. Kawabata, S., Matsuda, M., Tei, K., Hawai, H.: Experimental survey of the strain energy density function of isoprene rubber vulcanizate. *Macromolecules* **14**, 154–162 (1981). <https://doi.org/10.1021/ma50002a032>
41. Yeoh, O.H., Fleming, P.D.: A new attempt to reconcile the statistical and phenomenological theories of rubber elasticity. *J. Polym. Sci. Part B: Polym. Phys.* **35**(12), 1919–1931 (1997). [https://doi.org/10.1002/\(SICI\)1099-0488\(19970915\)35:12<1919::AID-POLB7>3.0.CO;2-K](https://doi.org/10.1002/(SICI)1099-0488(19970915)35:12<1919::AID-POLB7>3.0.CO;2-K)
42. Meunier, L., Chagnon, G., Favier, D., Orgéas, L., Vacher, P.: Mechanical experimental characterisation and numerical modelling of an unfilled silicone rubber. *Polym. Test.* **27**(6), 765–777 (2008). <https://doi.org/10.1016/j.polymertesting.2008.05.011>
43. Marckmann, G., Verron, E.: Comparison of hyperelastic models for rubber-like materials. *Rubber Chem. Technol.* **79**, 835–858 (2006)
44. Li, Y., Tang, S., Kröger, M., Liu, W.K.: Molecular simulation guided constitutive modeling on finite strain viscoelasticity of elastomers. *J. Mech. Phys. Solids* **88**, 204–226 (2016). <https://doi.org/10.1016/j.jmps.2015.12.007>

45. Marín, F., Martínez-Frutos, J., Ortigosa, R., Gil, A.J.: A convex multi-variable based computational framework for multilayered electro-active polymers. *Comput. Methods Appl. Mech. Eng.* **374**, 113567 (2021) <https://doi.org/10.1016/j.cma.2020.113567>
46. Lira, C., Innocenti, P., Scarpa, F.: Transverse elastic shear of auxetic multi re-entrant honeycombs. *Compos. Struct.* **90**(3), 314–322 (2009) <https://doi.org/10.1016/j.compstruct.2009.03.009>

Publisher's Note Springer Nature remains neutral with regard to jurisdictional claims in published maps and institutional affiliations.